

Excellent Carrier Transport Property of Hybrid Perovskites Sustained under High Pressures

Yanfeng Yin, Wenming Tian,* Hui Luo, Yuxiang Gao, Tingting Zhao, Chunyi Zhao, Jing Leng, Qi Sun, Jianbo Tang, Peng Wang, Quanjun Li, Xujie Lü, Jiming Bian,* and Shengye Jin*

HPSTAR
1328-2021



Cite This: *ACS Energy Lett.* 2022, 7, 154–161



Read Online

ACCESS |



Metrics & More

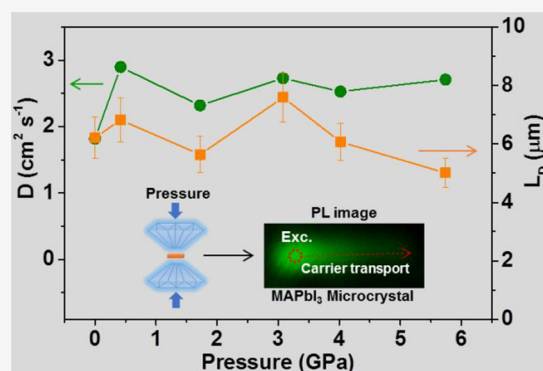


Article Recommendations



Supporting Information

ABSTRACT: High pressure treatment has become an effective way to tune the optical properties of halide perovskites. However, how compression can affect the carrier transport in perovskites remains unknown. Herein, by combining time-resolved imaging microscopy with a diamond anvil cell, we report *in situ* measurement of carrier transport in $\text{CH}_3\text{NH}_3\text{PbI}_3$ perovskite microcrystals (MCs) under high pressure. From ambient pressure to 5.7 GPa, the pressure induces a phase transition at 0.3–0.4 GPa and an isostructural phase transition at about 3 GPa. The carrier diffusivity is found to increase by at least 30% from $\sim 1.82 \text{ cm}^2 \text{ s}^{-1}$ at ambient pressure to $2.32\text{--}2.90 \text{ cm}^2 \text{ s}^{-1}$ at 0.4–5.7 GPa, leading to long carrier diffusion lengths of 5–8 μm . This result indicates that the perovskites can sustain excellent carrier transport properties under high pressure and thus enhances the potential of compression for optimizing the optoelectronic performance of perovskite materials.



Organic–inorganic metal halide perovskites are a family of semiconductor materials, attracting great attention for their tremendous applications in optoelectronic devices such as photovoltaics, light emitting diodes, and photodetectors.^{1–4} In parallel with the development of various perovskite-based devices, tuning or optimizing their optical and electronic properties by chemical composition adjustment (e.g., substitution or doping of chemical elements) or by the change of environmental conditions (e.g., temperature and pressure) has also become a subject under extensive investigation.^{5–8} Different from chemical composition adjustment, hydrostatic pressure is a straightforward and clean tool to tune the crystal structure and electronic wave functions by changing the lattice bond lengths and angles, which in turn alter materials' optical and electronic properties.^{9–16} In the past five years, pressure-induced structural, energetic, electronic, and optical properties of 3D perovskites (ABX_3 , where $\text{A} = \text{CH}_3\text{NH}_3^+$ (MA) or $\text{NH}_2\text{CHNH}_2^+$ (FA), $\text{B} = \text{metal cation}$, and $\text{X} = \text{Cl}^-, \text{Br}^-, \text{I}^-$) have been studied by many research groups through structural and spectroscopic measurements within a wide pressure tuning range up to 60 GPa.^{17–19,9,10,20–22,11,23–25} For example, Kong et al. reported band gap narrowing and carrier lifetime prolongation in MAPbX_3 perovskites under mid pressures (0–0.3 GPa), which was a change supposedly leading to improved perovskite photovoltaic performance.¹⁰ Furthermore, the apparent band gap closure and metallization of MAPbI_3 at ultrahigh pressure

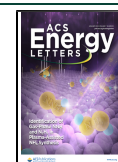
up to 60 GPa were also found.²² Recently, Shi et al. applied pressure (400–500 mbar) during the encapsulation of perovskite solar cells and found an improved photovoltaic performance.²⁶ These results indicate that a pressure treatment can significantly change the properties of perovskites. Note that applying high pressure to a realistic perovskite device is yet a great challenge. However, these high pressure related fundamental works can provide insights about how to maximize or tune the optical properties of perovskites, particularly when the pressure treatment can make a permanent change to the perovskites or the pressure-induced properties. It is worth mentioning that the effects observed in pressure experiments are expected to be reproduced through synthetic or chemical tuning.

In many perovskite optoelectronic devices, the carrier mobility (or diffusivity) and diffusion length are fundamental properties that determine the device performance.^{27,28} Therefore, understanding the change of these properties with compression is essential to evaluate the influence of pressure treatment on the optoelectronic performance of perovskites.

Received: October 31, 2021

Accepted: December 6, 2021

Published: December 8, 2021



Such measurements usually need to be carried out in a diamond anvil cell (DAC). The pressure-dependent carrier lifetime has been extensively investigated by combining the high pressure method with time-resolved photoluminescence (PL) and transient absorption techniques.^{10,21,29,5,30,24,31–33} However, limited by the small working space in a DAC and the inside pressure transmitting media, the measurements of charge mobility and diffusion length in a DAC are challenging when using traditional electrical techniques. Nevertheless, Jaffe et al. reported the conductivity of MAPbI₃ perovskites increased with compression up to 5 GPa and reached a plateau at 10 GPa.³⁴ Wang et al. also reported a decrease of conductivity of MAPbBr₃ with compression up to 25 GPa.¹⁷ However, these measurements only focused on the change of the electric properties of perovskites, but without considering their corresponding variation of optical property (e.g., carrier lifetime) with compression; therefore, their results are not directly relevant to the carrier transport of perovskites under high pressure. Furthermore, charge mobility measurement using tera Hertz (THz) spectroscopy also encounters significant signal disturbance caused by the optical reflection/diffraction from a DAC.³⁵ Therefore, how the photo-generated carrier diffusivity and diffusion length can change in perovskite materials under high pressure remains unknown.

Herein, by combining time-resolved and PL-scanned imaging microscopy with a DAC apparatus, we report a spectroscopic and *in situ* measurement of photoinduced carrier transport in MAPbI₃ perovskite microcrystals (MCs) under high pressure up to 5.7 GPa, when the perovskites retain a single crystal phase. The MAPbI₃ MCs are found to exhibit a tetragonal-to-cubic phase transition at 0.3–0.4 GPa and an isostructural phase transition at about 3 GPa as the pressure increases. Through the direct examination of carrier transport dynamics in a DAC, we find that the diffusion coefficient of perovskites shows an increase by more than 30% when the pressure is over 0.4 GPa. Combining the corresponding carrier lifetimes, the carrier diffusion length (L_D) is found to be from 5 to 8 μm under different pressures. This result suggests that the MAPbI₃ perovskites can sustain their excellent carrier transport properties under a pressure treatment (≤ 5.7 GPa), even though the pressure can cause significant structural defects to the crystal.

MAPbI₃ MCs were prepared by using the previously reported methods (see the Supporting Information for details).^{36,37} To investigate the structure change of MAPbI₃ MCs under pressure, we carried out *in situ* high pressure PXRD measurements on an ensemble of ground MCs in the procedure of compression (from 0 to 11.8 GPa) and decompression (Figure 1a). Consistent with the observations in previous reports,^{18,19,9,38–40,10,25} the first phase transition process is found to occur at about 0.3–0.4 GPa (Figure 1a), and the transition is identified to be from tetragonal to cubic phase through the Rietveld method of XRD data taken at 1 atm and 0.4 GPa (Figure S1). As the pressure is ≥ 4.6 GPa, a broad diffuse background at about 13.8° appears and some Bragg diffraction peaks disappear or become broad, indicating that the single crystals start to become amorphous and complete the amorphization before 11.8 GPa. Until now, a consensus is still lacking in the literature for the amorphization pressure of the MAPbI₃ perovskite. The start of amorphization at 2–3 GPa,^{39,40} 3–4 GPa,^{18,9} and >4 GPa^{19,38} pressures has been reported in different works. Upon decompression, the amorphous MAPbI₃ begins to recrystallize at 1.4 GPa and all

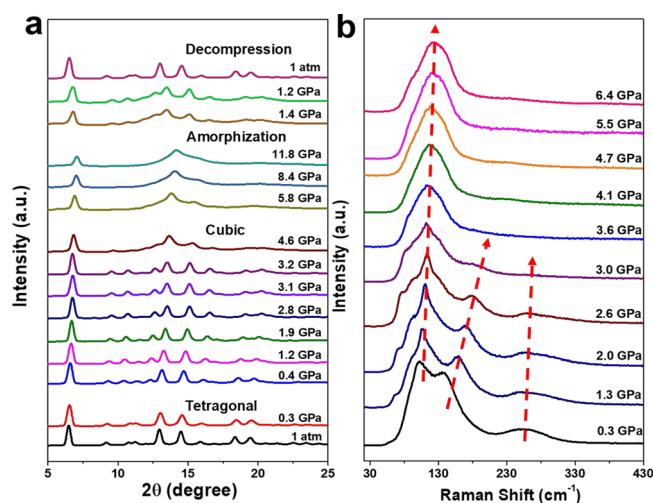


Figure 1. (a) XRD patterns of MAPbI₃ collected at different pressures up to 11.8 GPa and decompression. (b) Raman spectra of MAPbI₃ MCs at different pressures.

diffraction peaks re-emerge and eventually return to the original tetragonal phase at ambient conditions (Figure S2);^{18,19,38–40,10,25} this indicates that the phase transition in MAPbI₃ is totally reversible.

Besides the XRD measurement, we also collected the Raman spectra of MAPbI₃ MCs under different pressures (Figure 1b). According to the reported Raman spectra of MAPbI₃ at 1 atm, the band at 105 cm^{-1} can be assigned to stretching of the Pb–I bond, and the bands at 140 and 255 cm^{-1} are assigned to the libration and torsional modes of the MA cation, respectively.^{41,40} Note that the tetragonal-to-cubic phase transition at 0.3–0.4 GPa does not cause a prominent change in the Raman spectra; however, as the pressure increases to 3.0 GPa, the bands at 140 and 255 cm^{-1} almost disappear. This result indicates the vibration modes of the MA cation are significantly changed at this pressure point, although the crystals still remain in the cubic phase as shown in the XRD data. Furthermore, the PL intensity, lifetime (Figure 2), and UV–vis absorption spectra (Figure S3) also show an abrupt change at similar pressure (discussed later).

To elucidate the pressure-induced change at ~ 3 GPa, we analyze the lattice constant of MAPbI₃ MCs as a function of pressure and obtain the pressure–volume (P–V) correlation (Figure S4) based on the XRD data. The clear change of cell volume at about 3 GPa in the P–V plot, in combination with the abrupt changes in Raman, PL, and UV–vis absorption data under the same pressure, lead us to speculate that the MAPbI₃ MCs likely undergo an isostructural phase transition at about ~ 3 GPa.^{39,42,25} This type of phase transition was also reported in CsPbBr₃ perovskites and other materials, which is believed to originate from the electronic structural change, but without altering the XRD patterns.^{43,44,5,11,45,46}

To carry out the PL measurements on an individual MAPbI₃ MC under pressure, the as-synthesized MAPbI₃ MCs were transformed to a DAC apparatus coupled with a time-resolved imaging microscope (see Figure S5 for the setup). Figure 2a shows the optical images of a MC under different pressures (the ambient pressure is denoted as 0 GPa). The morphology of the MC is found unchanged, confirming that we measure the same MC at different pressures; however, at 7.7 GPa, the black MC turns red. This color change is caused by the abrupt

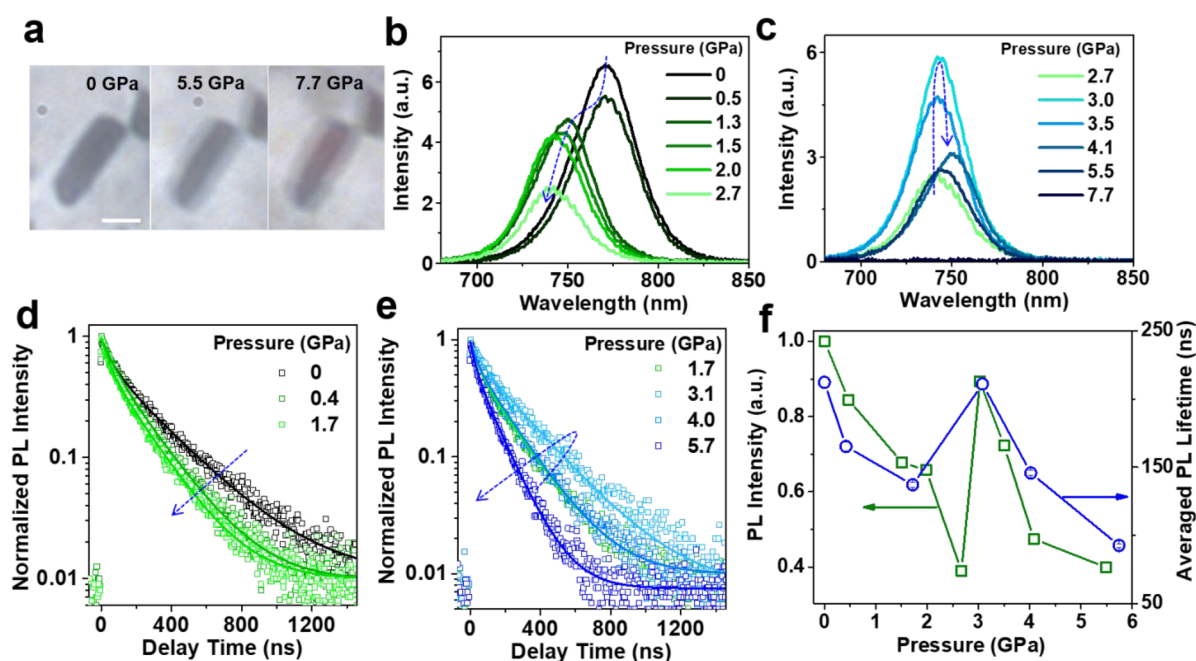


Figure 2. (a) Optical images of a MAPbI₃ MC at ambient pressure (0 GPa) and 5.5 and 7.7 GPa. The scale is 5 μm . (b and c) Pressure-dependent PL spectra of MAPbI₃ MCs under laser excitation at 405 nm. (d and e) TRPL kinetics of a MAPbI₃ MC under different pressures. Solid lines are the biexponential fits of the decay kinetics with the fitting parameters listed in Table S1. (f) Evolutions of the averaged PL lifetime and PL intensity as a function of pressure.

and large blue-shift in the absorption spectra of MCs as the pressure increases to >5 GPa (Figure S3), and within this high pressure range the MCs turn into an amorphous phase as confirmed in the XRD pattern (Figure 1a).¹⁸ For the MAPbI₃ perovskites, the amorphization process was found to start at different pressures, and this may relate to variations of the crystalline quality between MAPbI₃ fabricated by different methods.^{18,19,9,39,40} Before the investigation of carrier diffusivity under high pressure, we first carried out *in situ* PL measurements in the MCs to determine the pressure-induced change of carrier lifetime. In order to avoid laser damage to MCs, we use a low excitation density of 67 $\text{nJ cm}^{-2} \text{ pulse}^{-1}$. Figure 2 shows the PL spectra and time-resolved PL (TRPL) kinetics of a MAPbI₃ MC collected at different pressures in a DAC over a wide pressure range from 0 to 6 GPa. The steady-state PL intensity drops prominently as the pressure increases to 2.7 GPa, and a sharp recovery of PL is found at ~ 3 GPa, followed by a fast PL decrease as the pressure further increases (Figure 2b and c). Additional examples of PL spectral measurements in other MAPbI₃ MCs are shown in Figure S6, which repeat the similar PL variations at high pressures. Upon decompression, the PL spectrum completely reverts to its original state before compression, which excludes the effect of laser damage on the sample (Figure S7). Figure 2d and e exhibits the PL decay kinetics of the MC at different pressures, whose PL lifetimes are determined by fitting the kinetics with an exponential function (Table S1). The variation of the average PL lifetime as a function of pressure is well consistent with that of the PL intensity (Figure 2f). The abrupt change at ~ 3 GPa agrees with the change found in the Raman and P-V data and is attributed to the isostructural phase transition of the perovskite MC. Before and after the abrupt change at the pressure ~ 3 GPa, the increase of pressure significantly reduces the PL intensity and lifetime from ~ 200 ns to tens of nanoseconds.

Because the tetragonal-to-cubic phase transition occurs at 0.3–0.4 GPa, a detailed examination of the PL property from 0 to 1 GPa is also performed on an individual MAPbI₃ MC (Figure S8). The PL intensity and lifetime also show an abrupt increase when the phase transition occurs at 0.3–0.4 GPa, and other than this phase transition point, the increase of pressure causes large decreases of the PL intensity and lifetime.

The pressure-dependent PL intensity and lifetime of hybrid perovskites have been investigated by many research groups.^{10,29,47} Kong et al. reported that the pressure could first raise and then lower the PL lifetime of MAPbI₃ within the pressure range ≤ 2 GPa; such change was attributed to the formation of different trap states.¹⁰ However, Wang et al. also observed the reduction of carrier lifetime with the increase of pressure from ambient pressure to 0.3 GPa, which was explained by a pressure-induced reduction of the Rashba splitting and the energetic shift to a more direct band gap.²⁹ In this work, within the pressure tuning range up to 5.7 GPa, before and after the phase transition points, the drop of the PL lifetime is well consistent with that of PL intensity (Figure 2f), implying a pressure-induced increase of nonradiative carrier decay. Therefore, the decrease of carrier lifetime is likely due to the generation of more structural defects caused by pressure-induced lattice distortion. However, at the tetragonal-to-cubic phase transition point (0.3–0.4 GPa), the rearrangement of the lattice eliminates the pressure-induced structural defects, thus leading to the recovery of PL lifetime and intensity. The PL improvement at the isostructural phase transition point (~ 3 GPa) should be due to the change of the electronic band structure; however, the physical origin of the PL change at the isostructural phase transition for MAPbI₃ remains unknown and needs further experimental and theoretical investigations.

Given the carrier lifetime values under different pressures, the carrier diffusion length (L_D) can be calculated by $L_D = \sqrt{D\tau}$, where τ is the carrier lifetime and D is the carrier

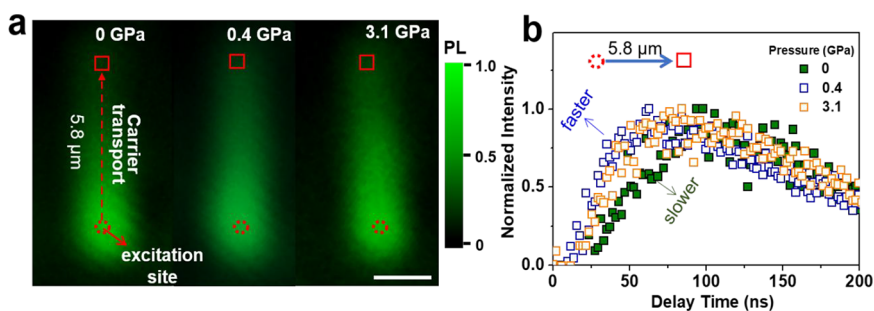


Figure 3. (a) Time-integrated PL intensity images of a MAPbI₃ MC collected at ambient pressure (0 GPa) and 0.4 and 3.1 GPa, showing the position of excitation and a distance of 5.8 μm from the excitation point. The scale is 2 μm. (b) Comparison of the carrier transport kinetics extracted at a position with a transport distance of 5.8 μm at ambient pressure (0 GPa) and 0.4 and 3.1 GPa.

diffusivity. To determine the diffusivity, we carried out a direct measurement on the carrier transport process in MAPbI₃ MCs in a DAC by using the time-resolved and PL-scanned imaging microscope (see Figure S5 for the setup), by which the visualization of the charge carrier transport in many nanostructured perovskite materials has been previously realized.^{37,48,49}

Figure 3a shows the time-integrated PL intensity images of a representative MAPbI₃ MC collected at ambient pressure (0 GPa), 0.4 GPa (tetragonal-to-cubic phase transition), and 3.1 GPa (isostructural phase transition). The MC was excited at a fixed position at one end of the MC by using a focused laser with a low excitation density of 61 nJ cm⁻² pulse⁻¹ to avoid laser damage. Meanwhile, at the pressure 5.7 GPa, the uniform PL intensity image and identical PL kinetics at different locations in the MC under homogeneous excitation further exclude any local laser damage to the MC (Figure S9). Because the PL intensity is positively proportional to the carrier density, the PL signal from any positions other than the excitation site indicates that the carriers diffuse away from the excitation spot and recombine along the transport pathway. Therefore, the carrier transport kinetics with a distance to the excitation spot can be extracted from the images. Figure 3b compares the carrier transport kinetics extracted at a position with a transport distance of 5.8 μm at 0 GPa, 0.4 GPa, and 3.1 GPa, and the comparisons of carrier transport kinetics at all examined pressures are shown in Figure S10. The kinetics at 0.4 and 3.1 GPa shows a faster rising process than that at 0 GPa, indicating that the pressure causes a faster carrier transport in the perovskite MC. Additional examples of carrier transport in MAPbI₃ MCs are shown in Figure S11, showing a similar increase of the carrier transport kinetics. Figure S10 exhibits a set of PL kinetics with different transport distances at different pressures. These kinetics can be described by a two-dimensional diffusion model:

$$\frac{\partial \phi(x, y, t)}{\partial t} = D \left\{ \frac{\partial^2 \phi(x, y, t)}{\partial x^2} + \frac{\partial^2 \phi(x, y, t)}{\partial y^2} \right\} + f(\phi(x, y, t)) \quad (1)$$

where $\phi(x, y, t)$ is the concentration of charge carriers at time t at position (x, y) ($0 \leq x \leq L_x$, $0 \leq y \leq L_y$; L_x and L_y are the side lengths of the crystal); D is the diffusion coefficient; and $f(\phi(x, y, t))$ is the charge recombination function. The boundary condition for the diffusion is defined as

$$\begin{aligned} \frac{\partial \phi^+(L_x, y, t)}{\partial x} &= \frac{\partial \phi^-(0, y, t)}{\partial x} = \frac{\partial \phi^+(x, L_y, t)}{\partial y} \\ &= \frac{\partial \phi^-(x, 0, t)}{\partial y} = 0 \end{aligned} \quad (2)$$

The + and - indicate the forward and backward first-order differential. The recombination of charge carriers can be described by a simple rate equation.

$$f(\phi(x, y, t)) = -k_1 \phi(x, y, t) - k_2 \phi(x, y, t)^2 \quad (3)$$

where k_2 is the radiative electron-hole recombination rate constant and k_1 is the defect-induced nonradiative carrier trapping rate constant. Moreover, we use the Gaussian function to describe the initial ($t = 0$) distribution of charge carriers at the excitation site:

$$\begin{aligned} \phi(x, y, 0)_{exc} &= \phi(x_0, y_0, 0) \\ &\exp \left(-2 \frac{(x - x_0)^2 + (y - y_0)^2}{r^2} \right) \end{aligned} \quad (4)$$

$$\int \phi(x, y, 0)_{exc} dx dy = \phi_0 \quad (5)$$

where $\phi(x_0, y_0, 0)$ is the carrier density at the center of the distribution; r is the radius of the distribution which is measured to be $\sim 0.64 \mu\text{m}$; and ϕ_0 is the total initial carrier density. Because eq 1 does not have a resolution, we perform the simulation of the carrier diffusion process in perovskite MCs using a home-built program. The side lengths of the MCs (L_x and L_y) and excitation site (x_0, y_0) were determined from the optical and PL intensity images. From this simulation, the change of the carrier density as a function of delay time at any position in the MC is determined. The PL intensity $I_{PL}(x, y, t)$ is proportional to $k_2 \phi(x, y, t)^2$.

With global fitting of these kinetics, the carrier diffusion coefficient is found to be $D = 2.73 \pm 0.033 \text{ cm}^2 \text{ s}^{-1}$ at 3.1 GPa, $2.90 \pm 0.036 \text{ cm}^2 \text{ s}^{-1}$ at 0.4 GPa, and $D = 1.82 \pm 0.024 \text{ cm}^2 \text{ s}^{-1}$ at 0 GPa. The diffusion coefficient obtained at 0 GPa is comparable to those previously reported in MAPbI₃ single crystals using different methods, implying that the diffusion coefficients measured at high pressure are reliable.^{28,50,51,37,52-54}

The results of measurements under other pressures are demonstrated in Figure S12. The carrier diffusivity measured at different pressures is summarized in Figure 4. At pressures from 0.4 to 5.7 GPa, the perovskite MCs all show a larger diffusivity by at least 30% than that at 0 GPa, and within the

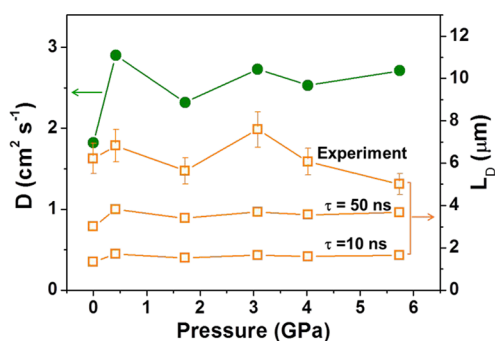


Figure 4. Carrier diffusivity (D) and diffusion length (L_D) of MAPbI₃ MCs measured at different pressures. Also exhibited are the simulated plots of L_D as a function pressure, assuming carrier lifetimes of $\tau = 50$ and 10 ns.

examined pressure range, the carrier diffusivity does not exhibit a significant variation.

In MAPbI₃ perovskites, the charge carriers have been known to diffuse in polarons because of the soft lattice and strong charge–phonon coupling, and their mobility can be estimated by $\mu = e\tau_s/m^*$, where e is the electronic charge, τ_s is the carrier scattering time, and m^* is the effective mass.^{55,56} We speculate that upon compression, the lattice of the perovskite becomes more rigid, and the size (thus the effective mass) of the polaron can become smaller; in addition, the more rigid lattice can also increase the carrier scattering time by reducing the phonon density. These pressure-induced changes should all lead to an increased mobility and thus a larger diffusivity.

Combining the lifetime data in Figure 2f, the carrier diffusion length (L_D) of MAPbI₃ MCs is calculated to be from 5 to 8 μm under different pressures via $L_D = \sqrt{D\tau}$ (Figure 4). The carrier diffusion length is about 6 μm at 0 GPa, which is comparable with the values in MAPbI₃ single crystals reported in others' and our previous works.^{50,57,54} The variation in diffusion length between different measurements is mainly caused by the variation of carrier lifetimes, by which the carrier diffusion length is calculated by $\sqrt{D\tau}$ (D is the diffusion coefficient and τ is the intrinsic carrier lifetime). The carrier lifetime in MAPbI₃ is usually limited by the quality (or density of trap states) in perovskites, which may vary significantly between samples synthesized by different methods. This remarkable L_D value at high pressure is owing to the increased diffusivity, which compensates the pressure-induced reduction of carrier lifetime, and the variation of L_D between different pressures is majorly caused by the change of carrier lifetime. Because the carrier diffusivity is determined by the lattice scattering rather than defect scattering, we believe that the high diffusivity value of MAPbI₃ can still be maintained even though the pressure has caused significant structural defects (thus shorter lifetimes).^{57,58} We therefore can estimate the diffusion length in a more serious case by assuming even smaller lifetimes of 10 or 50 ns and find decent L_D values of about 1 and 3 μm under different pressures (Figure 4). This result indicates that the pressure treatment does not make a fatal damage to the carrier transport in MAPbI₃ MCs because of the large D . Extending the result to the case of MAPbI₃ polycrystalline films whose lifetime is usually shorter than single crystals, we expect that compression may also be able to improve the intrinsic carrier diffusion (inner grain) in the polycrystalline perovskite films. However, applying high pressure in a realistic device is of great challenge,

and our results, from a fundamental point of view, may provide a potential pathway to improve the intrinsic carrier transport property of perovskite materials, particularly if the pressure effect can be reproduced or achieved by synthetic, chemical, or structural modification.

In summary, we have realized a direct observation of carrier transport in MAPbI₃ MCs under high pressure by combining a DAC apparatus with the time-resolved and PL-scanned imaging microscope. We demonstrated that the perovskite carrier lifetime changed significantly with the increase of pressure because of the pressure-induced structural defects and phase transition. However, the carrier diffusivity was increased by at least 30% within the examined pressure range of 0.4 to 5.7 GPa, which allowed the perovskites to maintain a long carrier diffusion length (5–8 μm). The result in this work sheds light on the influence of pressure on the carrier transport in MAPbI₃ perovskites and paves the way for the utilization of compression to tune or optimize the optoelectronic properties of perovskites.

■ ASSOCIATED CONTENT

Supporting Information

The Supporting Information is available free of charge at <https://pubs.acs.org/doi/10.1021/acsenerylett.1c02359>.

Experimental details; powder XRD, UV–vis absorption, and Raman spectra measurements; and additional results of measurements (PDF)

■ AUTHOR INFORMATION

Corresponding Authors

Wenming Tian – State Key Laboratory of Molecular Reaction Dynamics, Dalian Institute of Chemical Physics, Chinese Academy of Sciences, Dalian 116023, China; Email: tianwm@dicp.ac.cn

Jiming Bian – Key Laboratory of Materials Modification by Laser, Ion and Electron Beams (Ministry of Education), School of Physics, School of Microelectronics, Dalian University of Technology, Dalian 116024, China; orcid.org/0000-0002-4912-7606; Email: jmbian@dlut.edu.cn

Shengye Jin – State Key Laboratory of Molecular Reaction Dynamics, Dalian Institute of Chemical Physics, Chinese Academy of Sciences, Dalian 116023, China; orcid.org/0000-0003-2001-2212; Email: sjin@dicp.ac.cn

Authors

Yanfeng Yin – Key Laboratory of Materials Modification by Laser, Ion and Electron Beams (Ministry of Education), School of Physics, School of Microelectronics, Dalian University of Technology, Dalian 116024, China; State Key Laboratory of Molecular Reaction Dynamics, Dalian Institute of Chemical Physics, Chinese Academy of Sciences, Dalian 116023, China

Hui Luo – Center for High Pressure Science and Technology Advanced Research (HPSTAR), Shanghai 201203, China

Yuxiang Gao – State Key Laboratory of Superhard Materials, Jilin University, Changchun 130012, China

Tingting Zhao – State Key Laboratory of Superhard Materials, Jilin University, Changchun 130012, China

Chunyi Zhao – State Key Laboratory of Molecular Reaction Dynamics, Dalian Institute of Chemical Physics, Chinese Academy of Sciences, Dalian 116023, China

Jing Leng – State Key Laboratory of Molecular Reaction Dynamics, Dalian Institute of Chemical Physics, Chinese Academy of Sciences, Dalian 116023, China; orcid.org/0000-0002-8454-4835

Qi Sun – State Key Laboratory of Molecular Reaction Dynamics, Dalian Institute of Chemical Physics, Chinese Academy of Sciences, Dalian 116023, China; orcid.org/0000-0002-7092-0705

Jianbo Tang – State Key Laboratory of Molecular Reaction Dynamics, Dalian Institute of Chemical Physics, Chinese Academy of Sciences, Dalian 116023, China

Peng Wang – State Key Laboratory of Superhard Materials, Jilin University, Changchun 130012, China

Quanjun Li – State Key Laboratory of Superhard Materials, Jilin University, Changchun 130012, China; orcid.org/0000-0002-4718-4156

Xujie Lü – Center for High Pressure Science and Technology Advanced Research (HPSTAR), Shanghai 201203, China; orcid.org/0000-0001-8402-7160

Complete contact information is available at:
<https://pubs.acs.org/10.1021/acsenenergylett.1c02359>

Notes

The authors declare no competing financial interest.

ACKNOWLEDGMENTS

S. Jin acknowledges the funding support from the MOST (2018YFA0208704, 2016YFA0200602), NSFC (21725305), and the Strategic Priority Research Program of Chinese Academy of Sciences (XDB17010100). W. Tian acknowledges funding support from the NSFC (22073099) and Youth Innovation Promotion Association CAS (2019188). J. Bian acknowledges the funding support from NSFC (51872036, 51773025).

REFERENCES

- (1) Jeon, N. J.; Noh, J. H.; Yang, W. S.; Kim, Y. C.; Ryu, S.; Seo, J.; Seok, S. I. Compositional Engineering of Perovskite Materials for High-Performance Solar Cells. *Nature* **2015**, *517*, 476–480.
- (2) Yang, W. S.; Park, B. W.; Jung, E. H.; Jeon, N. J.; Kim, Y. C.; Lee, D. U.; Shin, S. S.; Seo, J.; Kim, E. K.; Noh, J. H.; Seok, S. I. Iodide Management in Formamidinium-Lead-Halide-Based Perovskite Layers for Efficient Solar Cells. *Science* **2017**, *356*, 1376–1379.
- (3) Yang, Z.; Deng, Y.; Zhang, X.; Wang, S.; Chen, H.; Yang, S.; Khurgin, J.; Fang, N. X.; Zhang, X.; Ma, R. High-Performance Single-Crystalline Perovskite Thin-Film Photodetector. *Adv. Mater.* **2018**, *30*, 1704333.
- (4) Chen, Z.; Li, Z.; Zhang, C.; Jiang, X. F.; Chen, D.; Xue, Q.; Liu, M.; Su, S.; Yip, H. L.; Cao, Y. Recombination Dynamics Study on Nanostructured Perovskite Light-Emitting Devices. *Adv. Mater.* **2018**, *30*, 1801370.
- (5) Xiao, G.; Cao, Y.; Qi, G.; Wang, L.; Liu, C.; Ma, Z.; Yang, X.; Sui, Y.; Zheng, W.; Zou, B. Pressure Effects on Structure and Optical Properties in Cesium Lead Bromide Perovskite Nanocrystals. *J. Am. Chem. Soc.* **2017**, *139*, 10087–10094.
- (6) Sun, Q.; Wang, S.; Zhao, C.; Leng, J.; Tian, W.; Jin, S. Excitation-Dependent Emission Color Tuning from an Individual Mn-Doped Perovskite Microcrystal. *J. Am. Chem. Soc.* **2019**, *141*, 20089–20096.
- (7) Li, Q.; Chen, Z.; Yang, B.; Tan, L.; Xu, B.; Han, J.; Zhao, Y.; Tang, J.; Quan, Z. Pressure-Induced Remarkable Enhancement of Self-Trapped Exciton Emission in One-Dimensional CsCu₂I₃ with Tetrahedral Units. *J. Am. Chem. Soc.* **2020**, *142*, 1786–1791.
- (8) Yin, Y.; Tian, W.; Leng, J.; Bian, J.; Jin, S. Carrier Transport Limited by Trap State in Cs₂AgBiBr₆ Double Perovskites. *J. Phys. Chem. Lett.* **2020**, *11*, 6956–6963.
- (9) Jaffe, A.; Lin, Y.; Beavers, C. M.; Voss, J.; Mao, W. L.; Karunadasa, H. I. High-Pressure Single-Crystal Structures of 3D Lead-Halide Hybrid Perovskites and Pressure Effects on Their Electronic and Optical Properties. *ACS Cent. Sci.* **2016**, *2*, 201–209.
- (10) Kong, L.; Liu, G.; Gong, J.; Hu, Q.; Schaller, R. D.; Dera, P.; Zhang, D.; Liu, Z.; Yang, W.; Zhu, K.; Tang, Y.; Wang, C.; Wei, S. H.; Xu, T.; Mao, H. K. Simultaneous Band-Gap Narrowing and Carrier-Lifetime Prolongation of Organic-Inorganic Trihalide Perovskites. *Proc. Natl. Acad. Sci. U. S. A.* **2016**, *113*, 8910–8915.
- (11) Zhang, L.; Zeng, Q.; Wang, K. Pressure-Induced Structural and Optical Properties of Inorganic Halide Perovskite CsPbBr₃. *J. Phys. Chem. Lett.* **2017**, *8*, 3752–3758.
- (12) Zhang, L.; Liu, C.; Wang, L.; Liu, C.; Wang, K.; Zou, B. Pressure-Induced Emission Enhancement, Band-Gap Narrowing, and Metallization of Halide Perovskite Cs₃Bi₂I₉. *Angew. Chem., Int. Ed.* **2018**, *57*, 11213–11217.
- (13) Liu, G.; Gong, J.; Kong, L.; Schaller, R. D.; Hu, Q.; Liu, Z.; Yan, S.; Yang, W.; Stoumpos, C. C.; Kanatzidis, M. G.; Mao, H.-k.; Xu, T. Isothermal Pressure-Derived Metastable States in 2D Hybrid Perovskites Showing Enduring Bandgap Narrowing. *Proc. Natl. Acad. Sci. U. S. A.* **2018**, *115*, 8076–8081.
- (14) Shi, Y.; Ma, Z.; Zhao, D.; Chen, Y.; Cao, Y.; Wang, K.; Xiao, G.; Zou, B. Pressure-Induced Emission (PIE) of One-Dimensional Organic Tin Bromide Perovskites. *J. Am. Chem. Soc.* **2019**, *141*, 6504–6508.
- (15) Zhang, L.; Liu, C.; Lin, Y.; Wang, K.; Ke, F.; Liu, C.; Mao, W. L.; Zou, B. Tuning Optical and Electronic Properties in Low-Toxicity Organic-Inorganic Hybrid (CH₃NH₃)₃Bi₂I₉ under High Pressure. *J. Phys. Chem. Lett.* **2019**, *10*, 1676–1683.
- (16) Zhang, L.; Fang, Y.; Sui, L.; Yan, J.; Wang, K.; Yuan, K.; Mao, W. L.; Zou, B. Tuning Emission and Electron–Phonon Coupling in Lead-Free Halide Double Perovskite Cs₂AgBiCl₆ under Pressure. *ACS Energy Lett.* **2019**, *4*, 2975–2982.
- (17) Wang, Y.; Lu, X.; Yang, W.; Wen, T.; Yang, L.; Ren, X.; Wang, L.; Lin, Z.; Zhao, Y. Pressure-Induced Phase Transformation, Reversible Amorphization, and Anomalous Visible Light Response in Organolead Bromide Perovskite. *J. Am. Chem. Soc.* **2015**, *137*, 11144–11149.
- (18) Wang, K.; Liu, R.; Qiao, Y.; Cui, J.; Song, B.; Liu, B.; Zou, B. Pressure-induced reversible phase transition and amorphization of CH₃NH₃PbI₃. **2015**, arXiv: 1509.03717.
- (19) Ou, T.; Yan, J.; Xiao, C.; Shen, W.; Liu, C.; Liu, X.; Han, Y.; Ma, Y.; Gao, C. Visible Light Response, Electrical Transport, and Amorphization in Compressed Organolead Iodine Perovskites. *Nanoscale* **2016**, *8*, 11426–11431.
- (20) Lu, X.; Wang, Y.; Stoumpos, C. C.; Hu, Q.; Guo, X.; Chen, H.; Yang, L.; Smith, J. S.; Yang, W.; Zhao, Y.; Xu, H.; Kanatzidis, M. G.; Jia, Q. Enhanced Structural Stability and Photo Responsiveness of C₃NH₃SnI₃ Perovskite Via Pressure-Induced Amorphization and Recrystallization. *Adv. Mater.* **2016**, *28*, 8663–8668.
- (21) Liu, G.; Kong, L.; Gong, J.; Yang, W.; Mao, H.-k.; Hu, Q.; Liu, Z.; Schaller, R. D.; Zhang, D.; Xu, T. Pressure-Induced Bandgap Optimization in Lead-Based Perovskites with Prolonged Carrier Lifetime and Ambient Retainability. *Adv. Funct. Mater.* **2017**, *27*, 1604208.
- (22) Jaffe, A.; Lin, Y.; Mao, W. L.; Karunadasa, H. I. Pressure-Induced Metallization of the Halide Perovskite (CH₃NH₃)PbI₃. *J. Am. Chem. Soc.* **2017**, *139*, 4330–4333.
- (23) Yin, T.; Fang, Y.; Chong, W. K.; Ming, K. T.; Jiang, S.; Li, X.; Kuo, J. L.; Fang, J.; Sum, T. C.; White, T. J.; Yan, J.; Shen, Z. X. High-Pressure-Induced Commutation and Recrystallization of CH₃NH₃PbBr₃ Nanocrystals as Large Thin Nanoplates. *Adv. Mater.* **2018**, *30*, 1705017.
- (24) Zhu, H.; Cai, T.; Que, M.; Song, J. P.; Rubenstein, B. M.; Wang, Z.; Chen, O. Pressure-Induced Phase Transformation and

Band-Gap Engineering of Formamidinium Lead Iodide Perovskite Nanocrystals. *J. Phys. Chem. Lett.* **2018**, *9*, 4199–4205.

(25) Liu, C.; Li, Z.; Yang, L.; Yao, X.; Li, H.; Liu, X.; Zhao, Y.; Zhu, P.; Cui, T.; Sun, C.; Bao, Y. Optical Behaviors of a Microsized Single-Crystal MAPbI₃ Plate under High Pressure. *J. Phys. Chem. C* **2019**, *123*, 30221–30227.

(26) Shi, L.; Zhang, M.; Cho, Y.; Young, T. L.; Wang, D.; Yi, H.; Kim, J.; Huang, S.; Ho-Baillie, A. W. Y. Effect of Pressing Pressure on the Performance of Perovskite Solar Cells. *ACS Appl. Energy Mater.* **2019**, *2*, 2358–2363.

(27) Stranks, S. D.; Eperon, G. E.; Grancini, G.; Menelaou, C.; Alcocer, M. J.; Leijtens, T.; Herz, L. M.; Petrozza, A.; Snaith, H. J. Electron-Hole Diffusion Lengths Exceeding 1 Micrometer in an Organometal Trihalide Perovskite Absorber. *Science* **2013**, *342*, 341–344.

(28) Dong, Q.; Fang, Y.; Shao, Y.; Mulligan, P.; Qiu, J.; Cao, L.; Huang, J. Solar Cells. Electron-Hole Diffusion Lengths > 175 μm in Solution-Grown CH₃NH₃PbI₃ Single Crystals. *Science* **2015**, *347*, 967–970.

(29) Wang, T.; Daiber, B.; Frost, J. M.; Mann, S. A.; Garnett, E. C.; Walsh, A.; Ehrler, B. Indirect to Direct Bandgap Transition in Methylammonium Lead Halide Perovskite. *Energy Environ. Sci.* **2017**, *10*, 509–515.

(30) Liu, X. C.; Han, J. H.; Zhao, H. F.; Yan, H. C.; Shi, Y.; Jin, M. X.; Liu, C. L.; Ding, D. J. Pressure Dependence of Excited-State Charge-Carrier Dynamics in Organolead Tribromide Perovskites. *Appl. Phys. Lett.* **2018**, *112*, 191903–191908.

(31) Liu, X.; Han, J.; Li, Y.; Cao, B.; Sun, C.; Yin, H.; Shi, Y.; Jin, M.; Liu, C.; Sun, M.; Ding, D. Ultrafast Carrier Dynamics in All-Inorganic CsPbBr₃ Perovskite across the Pressure-Induced Phase Transition. *Opt. Express* **2019**, *27*, 995–1003.

(32) Yuan, Y.; Liu, X. F.; Ma, X.; Wang, X.; Li, X.; Xiao, J.; Li, X.; Zhang, H. L.; Wang, L. Large Band Gap Narrowing and Prolonged Carrier Lifetime of (C₄H₉NH₃)₂PbI₄ under High Pressure. *Adv. Sci.* **2019**, *6*, 1900240.

(33) Liu, S.; Sun, S.; Gan, C. K.; Del Aguila, A. G.; Fang, Y.; Xing, J.; Do, T. T. H.; White, T. J.; Li, H.; Huang, W.; Xiong, Q. Manipulating Efficient Light Emission in Two-Dimensional Perovskite Crystals by Pressure-Induced Anisotropic Deformation. *Sci. Adv.* **2019**, *5*, 9445.

(34) Jaffe, A.; Lin, Y.; Karunadasa, H. I. Halide Perovskites under Pressure: Accessing New Properties through Lattice Compression. *ACS Energy Lett.* **2017**, *2*, 1549–1555.

(35) Eperon, G. E.; Leijtens, T.; Bush, K. A.; Prasanna, R.; Green, T.; Wang, J. T.; McMeekin, D. P.; Volonakis, G.; Milot, R. L.; May, R.; Palmstrom, A.; Slotcavage, D. J.; Belisle, R. A.; Patel, J. B.; Parrott, E. S.; Sutton, R. J.; Ma, W.; Moghadam, F.; Conings, B.; Babayigit, A.; Boyen, H. G.; Bent, S.; Giustino, F.; Herz, L. M.; Johnston, M. B.; McGehee, M. D.; Snaith, H. J. Perovskite-Perovskite Tandem Photovoltaics with Optimized Band Gaps. *Science* **2016**, *354*, 861–865.

(36) Fu, Y.; Meng, F.; Rowley, M. B.; Thompson, B. J.; Shearer, M. J.; Ma, D.; Hamers, R. J.; Wright, J. C.; Jin, S. Solution Growth of Single Crystal Methylammonium Lead Halide Perovskite Nanostructures for Optoelectronic and Photovoltaic Applications. *J. Am. Chem. Soc.* **2015**, *137*, 5810–5818.

(37) Tian, W.; Zhao, C.; Leng, J.; Cui, R.; Jin, S. Visualizing Carrier Diffusion in Individual Single-Crystal Organolead Halide Perovskite Nanowires and Nanoplates. *J. Am. Chem. Soc.* **2015**, *137*, 12458–12461.

(38) Jiang, S.; Fang, Y.; Li, R.; Xiao, H.; Crowley, J.; Wang, C.; White, T. J.; Goddard, W. A., III; Wang, Z.; Baikie, T.; Fang, J. Pressure-Dependent Polymorphism and Band-Gap Tuning of Methylammonium Lead Iodide Perovskite. *Angew. Chem., Int. Ed.* **2016**, *55*, 6540–6544.

(39) Szafranski, M.; Katrusiak, A. Mechanism of Pressure-Induced Phase Transitions, Amorphization, and Absorption-Edge Shift in Photovoltaic Methylammonium Lead Iodide. *J. Phys. Chem. Lett.* **2016**, *7*, 3458–3466.

(40) Capitani, F.; Marini, C.; Caramazza, S.; Postorino, P.; Garbarino, G.; Hanfland, M.; Pisanu, A.; Quadrelli, P.; Malavasi, L. High-Pressure Behavior of Methylammonium Lead Iodide (MAPbI₃) Hybrid Perovskite. *J. Appl. Phys.* **2016**, *119*, 185901–185906.

(41) Pérez-Osorio, M. A.; Milot, R. L.; Filip, M. R.; Patel, J. B.; Herz, L. M.; Johnston, M. B.; Giustino, F. Vibrational Properties of the Organic–Inorganic Halide Perovskite CH₃NH₃PbI₃ from Theory and Experiment: Factor Group Analysis, First-Principles Calculations, and Low-Temperature Infrared Spectra. *J. Phys. Chem. C* **2015**, *119*, 25703–25718.

(42) Szafranski, M.; Katrusiak, A. Photovoltaic Hybrid Perovskites under Pressure. *J. Phys. Chem. Lett.* **2017**, *8*, 2496–2506.

(43) Jaffe, A.; Lin, Y.; Mao, W. L.; Karunadasa, H. I. Pressure-induced conductivity and yellow-to-black piezochromism in a layered Cu-Cl hybrid perovskite. *J. Am. Chem. Soc.* **2015**, *137*, 1673–1678.

(44) Wang, L.; Wang, K.; Xiao, G.; Zeng, Q.; Zou, B. Pressure-Induced Structural Evolution and Band Gap Shifts of Organometal Halide Perovskite-Based Methylammonium Lead Chloride. *J. Phys. Chem. Lett.* **2016**, *7*, 5273–5279.

(45) Zhang, L.; Wang, L.; Wang, K.; Zou, B. Pressure-Induced Structural Evolution and Optical Properties of Metal-Halide Perovskite CsPbCl₃. *J. Phys. Chem. C* **2018**, *122*, 15220–15225.

(46) Ma, Z.; Li, F.; Qi, G.; Wang, L.; Liu, C.; Wang, K.; Xiao, G.; Zou, B. Structural stability and optical properties of two-dimensional perovskite-like CsPb₂Br₅ microplates in response to pressure. *Nanoscale* **2019**, *11*, 820–825.

(47) Yin, T.; Liu, B.; Yan, J.; Fang, Y.; Chen, M.; Chong, W. K.; Jiang, S.; Kuo, J. L.; Fang, J.; Liang, P.; Wei, S.; Loh, K. P.; Sum, T. C.; White, T. J.; Shen, Z. X. Pressure-Engineered Structural and Optical Properties of Two-Dimensional (C₄H₉NH₃)₂PbI₄ Perovskite Exfoliated nm-Thin Flakes. *J. Am. Chem. Soc.* **2019**, *141*, 1235–1241.

(48) Tian, W.; Cui, R.; Leng, J.; Liu, J.; Li, Y.; Zhao, C.; Zhang, J.; Deng, W.; Lian, T.; Jin, S. Limiting Perovskite Solar Cell Performance by Heterogeneous Carrier Extraction. *Angew. Chem., Int. Ed.* **2016**, *55*, 13067–13071.

(49) Zhao, C.; Tian, W.; Sun, Q.; Yin, Z.; Leng, J.; Wang, S.; Liu, J.; Wu, K.; Jin, S. Trap-Enabled Long-Distance Carrier Transport in Perovskite Quantum Wells. *J. Am. Chem. Soc.* **2020**, *142*, 15091–15097.

(50) Saidaminov, M. I.; Abdelhady, A. L.; Murali, B.; Alarousu, E.; Burlakov, V. M.; Peng, W.; Dursun, I.; Wang, L.; He, Y.; Maculan, G.; Goriely, A.; Wu, T.; Mohammed, O. F.; Bakr, O. M. High-quality bulk hybrid perovskite single crystals within minutes by inverse temperature crystallization. *Nat. Commun.* **2015**, *6*, 7586.

(51) Shi, D.; Adinolfi, V.; Comin, R.; Yuan, M.; Alarousu, E.; Buin, A.; Chen, Y.; Hoogland, S.; Rothenberger, A.; Katsiev, K.; Losovyj, Y.; Zhang, X.; Dowben, P. A.; Mohammed, O. F.; Sargent, E. H.; Bakr, O. M. Solar cells. Low trap-state density and long carrier diffusion in organolead trihalide perovskite single crystals. *Science* **2015**, *347*, 519–522.

(52) Adinolfi, V.; Yuan, M.; Comin, R.; Thibau, E. S.; Shi, D.; Saidaminov, M. I.; Kanjanaboos, P.; Kopilovic, D.; Hoogland, S.; Lu, Z. H.; Bakr, O. M.; Sargent, E. H. The In-Gap Electronic State Spectrum of Methylammonium Lead Iodide Single-Crystal Perovskites. *Adv. Mater.* **2016**, *28*, 3406–3410.

(53) Tian, W.; Leng, J.; Zhao, C.; Jin, S. Long-Distance Charge Carrier Funneling in Perovskite Nanowires Enabled by Built-in Halide Gradient. *J. Am. Chem. Soc.* **2017**, *139*, 579–582.

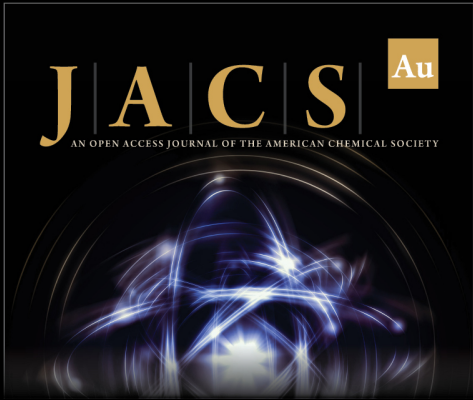
(54) Ščajevo, P.; Miasojedovas, S.; Juršenas, S. A carrier density dependent diffusion coefficient, recombination rate and diffusion length in MAPbI₃ and MAPbBr₃ crystals measured under one- and two-photon excitations. *J. Mater. Chem. C* **2020**, *8*, 10290–10301.

(55) Herz, L. M. Charge-Carrier Mobilities in Metal Halide Perovskites: Fundamental Mechanisms and Limits. *ACS Energy Lett.* **2017**, *2*, 1539–1548.


(56) Zhou, L.; Katan, C.; Nie, W.; Tsai, H.; Pedesseau, L.; Crochet, J. J.; Even, J.; Mohite, A. D.; Tretiak, S.; Neukirch, A. J. Cation Alloying Delocalizes Polarons in Lead Halide Perovskites. *J. Phys. Chem. Lett.* **2019**, *10*, 3516–3524.


(57) Miyata, K.; Atallah, T. L.; Zhu, X. Y. Lead halide perovskites: Crystal-liquid duality, phonon glass electron crystals, and large polaron formation. *Sci. Adv.* **2017**, *3*, 1701469.


(58) Zhao, C.; Sun, Q.; Cui, R.; Leng, J.; Tian, W.; Jin, S. Carrier diffusion coefficient is independent of defects in $\text{CH}_3\text{NH}_3\text{PbBr}_3$ single crystals: Direct evidence. *J. Energy Chem.* **2021**, *58*, 441–445.



JACS Au
AN OPEN ACCESS JOURNAL OF THE AMERICAN CHEMICAL SOCIETY

 Editor-in-Chief
Prof. Christopher W. Jones
Georgia Institute of Technology, USA

Open for Submissions 

pubs.acs.org/jacsau  ACS Publications
Most Trusted. Most Cited. Most Read.